Ab initio calculations for the transport properties of metals within Boltzmann transport theory: From equilibrium to nonequilibrium heating regime

N. A. Smirnov *

Federal State Unitary Enterprise, Russian Federal Nuclear Center - Zababakhin All-Russian Research Institute of Technical Physics, 456770 Snezhinsk, Russia

(Received 26 April 2022; revised 6 July 2022; accepted 12 July 2022; published 22 July 2022)

The paper offers an approach to *ab initio* calculations for predicting the electron transport properties of solid-state metals in a case of nonequilibrium heating. Formulas for the electrical resistivity (also static conductivity) and thermal conductivity of metals at different electron and lattice temperatures were derived within a method proposed by Allen [Phys. Rev. B **17**, 3725 (1978)] for the solution of the Boltzmann transport equation. The approach works well under equilibrium heating too when electron and lattice temperatures are equal. It performs most effectively if it is necessary to allow for the Fermi smearing of the electron distribution function over quantum states and the energy dependence of the electron-phonon spectral function. Four metals—Cu, Ag, Au and Pd—are considered as examples. We succeeded to reproduce well the temperature dependencies of electrical resistivity and thermal conductivity of studied metals in a wide range of temperatures under equilibrium heating. For the nonequilibrium regime of heating, calculations reproduce quite well the temporal evolution of the static electrical conductivity of gold, observed in recent experiments for the interaction of thin gold foils with ultrashort laser pulses.

DOI: 10.1103/PhysRevB.106.024109

I. INTRODUCTION

The study for the transport properties of matter has been of unflagging interest among researchers in various areas of physics for several decades. The important steps in their calculation for solid metals from first principles within density functional theory (DFT) were made in a series of papers [1–6]. The papers describe a method to solve the linearized Boltzmann transport equation (BTE) [2–4] and its particular implementation with the use of the state-of-the-art full-potential [5] and pseudopotential [6] band structure calculation methods. For the linearized BTE, the authors of Refs. [3,4] propose an approach based on the lowest-order variational approximation (LOVA). The scattering operator and the electron distribution function are presented as an expansion in terms of basis functions composed of products of Fermi-surface harmonics and energy-dependent polynomials. After some simplifications (neglecting Fermi smearing and the energy dependence of the electron-phonon spectral function), the calculation of electrical resistivity ρ and electron thermal conductivity κ_e reduces to one-dimensional integration where the integrand includes the electron-phonon spectral function defined at the Fermi energy [4]. Calculations [5,6] show that even such an approximate approach helps attain good agreement between calculated and experimental ρ and κ_e for a number of metals at temperatures $T \lesssim 300$ K.

Results of calculations for the transport properties of metals utilizing a more general formula [3] within the LOVA approximation has recently been demonstrated in papers [7,8], where the above mentioned simplifications were not used. The authors succeeded to reproduce rather well the experimental temperature dependencies of electrical resistivity and Seebeck coefficient for a series of metals even at high temperatures, which is not always possible to do with more rough approximation [4]. Unfortunately, in papers [7,8] the thermal conductivity of the studied metals was not calculated, which would have made it possible to more fully judge about the success of their approach.

On the other hand, alternative methods for solving BTE through calculations from first principles both for metals and for semiconductors have recently appeared (see, for example, [9–13]). Besides the approaches that use well-known relaxation time approximation in different variants [11–13], the linearized Boltzmann equation can be solved by iterations [9], starting from an initial approximation, which is taken to be the relaxation time approximation. These papers mainly deal with low temperatures ($10 < T \lesssim 300$ K) where the accurate account of inelastic electron-phonon scattering is needed to attain good agreement with experiment.

Another method often used for determining the transport properties in DFT calculations is based on the Kubo-Greenwood formula [14] that allows the electrical conductivity of material to be determined in the approximation of linear response to an external electric field. Having calculated the Onsager coefficients, one can obtain the other transport quantities. This approach is intensively used to study the properties of solids and melts [15–17], as well as the properties of warm dense matter (WDM) [18–22] where density is comparable with or higher than the solid-state density under ambient conditions and the temperature may reach a few electron volts. The Kubo-Greenwood formula enables calculation of the real

* nasmirnov@vniitf.ru

part of conductivity σ as a function of frequency ω of a time-dependent field. When used with the Kramers–Kronig relation, it eventually gives the dynamic conductivity (AC conductivity) of matter. Also, this formula is often used to determine the electrical conductivity and optical properties of materials with different electron T_e, and ion T_i, temperatures, i.e., for the two-temperature WDM heating. Such a nonequilibrium state occurs after irradiation of material by ultrashort laser pulses with duration $\tau_p \sim 100$ fs. Under these extreme conditions, none of the contact electrical probes is applicable to measure electrical conductivity. Therefore, until recently the measurable quantity in ultrashort laser interaction experiments was AC conductivity that could be found via the measured reflectivity and transmissivity of the probe laser pulse. However, an experiment [23] has been taken quite recently, where the static conductivity (DC conductivity) was directly measured in thin gold foils after irradiation by femtosecond laser pulses. That was accomplished with an ultrafast terahertz probe pulse. The terahertz pulse characteristics varying slowly relative to the time scale of the electron-ion interaction were chosen such as to allow static electrical conductivity measurements [23]. Additional experimental data on DC conductivity, *inter alia*, help verify different models intended to calculate only the static transport properties [24,25] and where some parameters have to be determined empirically. In practice, DC conductivity can be found by extrapolating the real part of dynamic conductivity to zero frequency ω, but with account for the finite experimental accuracy, this might lead to an uncontrolled error.

The evolution of nonequilibrium heated material is usually described with a two-temperature model [26,27]. To determine the temperature variation of the electron and ion subsystems in the irradiated foil with time, a system of equations is solved, which includes the temperature dependence of the electron thermal conductivity as one of the parameters. Knowledge of the dependence κ_e on T_e and T_i is needed, for example, for successful simulation of ablation since the κ_e value defines heat diffusion into deeper parts of the material from its surface. Usually the behavior of the function $\kappa_e(T_e, T_i)$ is determined with the help of various semi-empirical and model representations [27–32]. For example, at low temperatures, Drude theory is used with coefficients adjusted against low-temperature experimental data, and the hot plasma limit (Spitzer theory) is utilized for high temperatures. The required wide-range dependence $\kappa_e(T_e, T_i)$ results from interpolation between these two limits. From the standpoint of accuracy, there however exists an intermediate range of temperatures (at least a few electron volts) where this interpolation may become a source of inaccuracies. Since it is difficult to obtain experimental data in this temperature range, the lack of information can be balanced by calculations from first principles, which are accurate enough to determine different properties of matter.

As shown in experiments [23,33], even at ultrashort pulse intensities of $\sim 10^{12}\ W/cm^2$, the crystal structure of some metals is preserved after irradiation during a rather long time ($\gtrsim 10$ ps) compared with pulse duration ($\sim$100 fs). At the same time, the difference between lattice and electron temperatures reaches a few tens of times [23,33]. Later the electron-phonon interaction leads to a gradual equalization of temperatures in the system and, possibly, to the destruction of the crystal structure. Thus, calculation of the transport properties of crystalline matter under nonequilibrium heating is quite a live issue.

In this paper, we rewrite the solution of the linearized Boltzmann equation for the case of nonequilibrium heating using a method proposed by Allen [3]. Introducing some approximations, which weakly affect calculation accuracy, we derive formulas for electrical resistivity (also DC conductivity) and thermal conductivity of metals, which can be implemented in modern first-principles codes. Our implementation is done within the all-electron FP-LMTO method. The obtained formulas are universal and can also be used in the case of equilibrium heating where the electron and lattice temperatures are equal. Additionally, we consider the case of elastic scattering, which is of interest at rather high temperatures (above the Debye temperatures Θ_D). The proposed method for calculating the transport properties of two-temperature warm dense matter is an alternative to the Kubo-Greenwood method for crystals and has certain advantages. The next section provides the theory with derivation of necessary formulas and gives a description of parameters for *ab initio* calculations. Section III presents comparison between calculated and experimental results for four metals—Cu, Ag, Au, and Pd—for the case of $T_e = T_i$ (at temperatures from about 30 K up to melting) and the case of $T_e \neq T_i$ where the electron temperature increases up to 23 kK (about 2 eV) while the lattice remains relatively cold. In addition, the section provides comparison with the semi-empirical dependence of thermal conductivity $\kappa_e \sim T_e$ often used in two-temperature calculations at relatively low temperatures. The last section briefly summarizes results of this paper.

II. THEORY AND CALCULATION METHOD

A. Solution of the Boltzmann transport equation

Let us briefly describe the method of solving the linearized Boltzmann transport equation, proposed in Ref. [3]. Assume that $T_e \neq T_i$, i.e., the system consists of electrons and ions, which have different temperatures. If the system is under the action of an external uniform electric field $\vec{E}$ (the magnetic field is neglected) and a uniform thermal gradient $\vec{\nabla} T_e$, then the electron transport properties can be determined from the equation [3,14]

$$\left(\frac{\varepsilon_{\mathbb{k}}}{T_e}\vec{\nabla} T_e + e\vec{E}\right)\vec{v}_{\mathbb{k}}\frac{\partial f(\varepsilon_{\mathbb{k}})}{\partial \varepsilon_{\mathbb{k}}} = \sum_{\mathbb{k}'} Q_{\mathbb{k}\mathbb{k}'}\phi_{\mathbb{k}'}. \tag{1}$$

Here $\vec{v}_{\mathbb{k}} = (1/\hbar)\vec{\nabla}_{\mathbb{k}}\varepsilon_{\mathbb{k}}$ is the velocity of electrons with energy $\varepsilon_{\mathbb{k}}$ ($\varepsilon_{\mathbb{k}}$ determined relative to the chemical potential μ), $\mathbb{k}$ is short for $(\vec{k}\mathrm{j})$, wave number and band index, $f(\varepsilon_{\mathbb{k}})$ is the Fermi-Dirac distribution function, $f(\varepsilon_{\mathbb{k}}) = 1/[1 + \exp(f(\varepsilon_{\mathbb{k}})/k_B T_e)]$, and e is the electron charge. The right-hand side of Eq. (1) has the scattering operator $Q_{\mathbb{k}\mathbb{k}'}$ multiplied by a function $\phi_{\mathbb{k}'}$, which is smooth in energy. Equation (1) is written in the assumption that the electron distribution $\Phi_{\mathbb{k}}$ in the presence of perturbation can be expanded

to the linear term as

$$\Phi_{\mathbb{k}} = f(\varepsilon_{\mathbb{k}}) + \phi_{\mathbb{k}}\left(-\frac{\partial f(\varepsilon_{\mathbb{k}})}{\partial \varepsilon_{\mathbb{k}}}\right). \tag{2}$$

With this form of the electron distribution function, expressions for electrical and thermal currents are written as

$$\vec{j}_e = -2e\sum_{\mathbb{k}} \vec{v}_{\mathbb{k}}\phi_{\mathbb{k}}\left(-\frac{\partial f}{\partial \varepsilon_{\mathbb{k}}}\right) = \beta_{00}\vec{E} + \beta_{01}\vec{\nabla}T_e, \tag{3}$$

$$\vec{j}_Q = 2\sum_{\mathbb{k}} \varepsilon_{\mathbb{k}}\vec{v}_{\mathbb{k}}\phi_{\mathbb{k}}\left(-\frac{\partial f}{\partial \varepsilon_{\mathbb{k}}}\right) = \beta_{10}\vec{E} + \beta_{11}\vec{\nabla}T_e, \tag{4}$$

where the factors of 2 are for spin degeneracy. Here the coefficients β_{ij} are related to the transport coefficients: electrical conductivity is $\sigma = \beta_{00}$ and thermal conductivity is $\kappa_e = -\beta_{11} + \beta_{10}\beta_{00}^{-1}\beta_{01}$, where the second summand expresses the thermoelectric contribution [3]. Beta coefficients are related to Onsager coefficients as $\beta_{00} = L_{11}$, $\beta_{01} = -L_{12}$, $\beta_{10} = L_{21}$, $\beta_{11} = -L_{22}$.

Let both $\vec{E}$ and $\vec{\nabla}T_e$ point in one of the directions $\alpha = x, y, z$ of Cartesian coordinates. For solving Eq. (1), Allen introduces the following doubled set of basis functions:

$$\chi_{\alpha\zeta}(\mathbb{k}) = \frac{F_\alpha(\mathbb{k})\eta_\zeta(\varepsilon_{\mathbb{k}})}{N(\varepsilon_{\mathbb{k}})\upsilon(\varepsilon_{\mathbb{k}})}, \tag{5}$$

$$\gamma_{\alpha\zeta}(\mathbb{k}) = F_\alpha(\mathbb{k})\eta_\zeta(\varepsilon_{\mathbb{k}})\upsilon(\varepsilon_{\mathbb{k}})\left(-\frac{\partial f}{\partial \varepsilon_{\mathbb{k}}}\right). \tag{6}$$

Here $F_\alpha(\mathbb{k}) = \upsilon_\alpha(\mathbb{k})/\upsilon(\varepsilon_{\mathbb{k}})$ are surface harmonics being simply normalized electron velocities [2]. Functions (5) and (6) are cell periodic because velocities are cell periodic. The normalization factor $\upsilon(\varepsilon) \equiv \langle \upsilon_\alpha^2(\varepsilon)\rangle^{1/2}$, which is the root-mean-square velocity in direction α of an electron with energy ε is found as

$$N(\varepsilon)\langle \upsilon_\alpha^2(\varepsilon)\rangle = \sum_{\mathbb{k}} \upsilon_\alpha^2(\mathbb{k})\delta(\varepsilon_{\mathbb{k}} - \varepsilon), \tag{7}$$

where $N(\varepsilon)$ is the electron density of states per spin. As seen from Eq. (7), velocity normalization to the electronic DOS leads to singularity in calculations for semiconductors. For semiconductors, this approach will only work if doping is used, so that the chemical potential gets into the valence or conduction band.

The functions $\eta_\zeta(\varepsilon)$ are energy-dependent polynomials orthonormalized with weight function $-\partial f/\partial\varepsilon$,

$$\int_{-\infty}^{\infty}\left(-\frac{\partial f}{\partial \varepsilon}\right)\eta_\zeta(\varepsilon)\eta_{\zeta'}(\varepsilon)d\varepsilon = \delta_{\zeta\zeta'}. \tag{8}$$

Like Allen, we will only use the first two polynomials, $\eta_0 = 1$, $\eta_1(\varepsilon) = \sqrt{3}\varepsilon/(\pi k_B T_e)$, and this seems to be quite an accurate approximation giving well converging results at $T_e = T_i$ [7,8]. In the case of nonequilibrium heating, we can also expect good calculation accuracy because, as shown in our first-principles calculations, the values of μ for the considered metals are of the order of 10^2 kK, which is much higher than the temperatures $T_e \sim 10$ kK we are considering and the electron subsystem can be regarded as sufficiently degenerate. Thus, the surface harmonics effectively solve the angular part of the problem, while the energy polynomials solve its "radial" part [3].

The functions $F_\alpha(\mathbb{k})$ are orthonormalized according to the rule

$$\frac{1}{N(\varepsilon)}\sum_{\mathbb{k}} F_\alpha(\mathbb{k})F_{\alpha'}(\mathbb{k})\delta(\varepsilon_{\mathbb{k}} - \varepsilon) = \delta_{\alpha\alpha'}, \tag{9}$$

and basis functions (5) and (6) possess the following useful properties:

$$\sum_{\mathbb{k}} \chi_{\alpha\zeta}(\mathbb{k})\gamma_{\alpha'\zeta'}(\mathbb{k}) = \delta_{\alpha\alpha'}\delta_{\zeta\zeta'}, \tag{10}$$

$$\sum_{\alpha'\zeta'} \chi_{\alpha'\zeta'}(\mathbb{k}')\gamma_{\alpha'\zeta'}(\mathbb{k}'') = \delta_{\mathbb{k}'\mathbb{k}''}. \tag{11}$$

Our goal is to determine, with use of basis functions (5) and (6), the scattering operator $Q_{\mathbb{k}\mathbb{k}'}$ required for the further calculation of transport properties. Note that $\chi_{\alpha\zeta}$ is convenient for expanding functions, which are smooth in energy, such as $\phi_{\mathbb{k}}$, while $\gamma_{\alpha\zeta}$ is convenient for the scattering operator that peaks at $\varepsilon = \mu$. Expressing the left-hand side of Eq. (1) in terms of the functions $\gamma_{\alpha\zeta}$, where ζ =0,1, we obtain

$$-eE\gamma_{\alpha 0}(\mathbb{k}) - (\pi k_B/\sqrt{3})\nabla T_e\gamma_{\alpha 1}(\mathbb{k}). \tag{12}$$

If multiply Eq. (1) by $\chi_{\alpha\zeta}$ and sum over $\mathbb{k}$ using expression (10) for the left-hand side and expression (11) for the right-hand one, then the Boltzmann equation takes the form

$$-eE\delta_{\zeta 0} - (\pi k_B/\sqrt{3})\nabla T_e\delta_{\zeta 1} = \sum_{\alpha'\zeta'} Q_{\alpha\zeta,\alpha'\zeta'}\phi_{\alpha'\zeta'}. \tag{13}$$

$Q_{\alpha\zeta,\alpha'\zeta'}$ and $\phi_{\alpha\zeta}$ are determined as

$$Q_{\alpha\zeta,\alpha'\zeta'} = \sum_{\mathbb{k}\mathbb{k}'} \chi_{\alpha\zeta}(\mathbb{k})Q_{\mathbb{k}\mathbb{k}'}\chi_{\alpha'\zeta'}(\mathbb{k}'), \quad \phi_{\alpha\zeta} = \sum_{\mathbb{k}} \gamma_{\alpha\zeta}(\mathbb{k})\phi_{\mathbb{k}}. \tag{14}$$

Using (11), we can also obtain the inverse relations

$$Q_{\mathbb{k}\mathbb{k}'} = \sum_{\alpha\zeta,\alpha'\zeta'} \gamma_{\alpha\zeta}(\mathbb{k})Q_{\alpha\zeta,\alpha'\zeta'}\gamma_{\alpha'\zeta'}(\mathbb{k}'), \quad \phi_{\mathbb{k}} = \sum_{\alpha\zeta} \phi_{\alpha\zeta}\chi_{\alpha\zeta}(\mathbb{k}). \tag{15}$$

Now rewrite expressions (3) and (4) for currents in the direction α, using the introduced basis functions,

$$j_e = -2e\phi_{\alpha 0}, \tag{16}$$

$$j_Q = (2\pi k_B T_e/\sqrt{3})\phi_{\alpha 1}. \tag{17}$$

The scattering operator is written as the difference of two parts allowing for scattering from state $\mathbb{k}$ into state $\mathbb{k}'$ (scattering-out process) and from state $\mathbb{k}'$ into state $\mathbb{k}$ (scattering-in process) [14]. After its linearization in the conventional way with account for the energy conservation and the principle of detailed balance, it can be expressed in terms of the equilibrium transition probability $P_{\mathbb{k}\mathbb{k}'}$ as [14,34]

$$Q_{\mathbb{k}\mathbb{k}'} = Q^{\text{out}}_{\mathbb{k}\mathbb{k}'} - Q^{in}_{\mathbb{k}\mathbb{k}'} = \frac{1}{k_B T_e}\left(\delta_{\mathbb{k}\mathbb{k}'}\sum_{\mathbb{k}''} P_{\mathbb{k}\mathbb{k}''} - P_{\mathbb{k}\mathbb{k}'}\right). \tag{18}$$

Then $Q_{\alpha\zeta,\alpha'\zeta'}$ from (14) can be rewritten in the following form:

$$Q_{\alpha\zeta,\alpha'\zeta'} = \frac{1}{2k_B T_e}\sum_{\mathbb{k}\mathbb{k}'} P_{\mathbb{k}\mathbb{k}'}[\chi_{\alpha\zeta}(\mathbb{k}) - \chi_{\alpha\zeta}(\mathbb{k}')] \times [\chi_{\alpha'\zeta'}(\mathbb{k}) - \chi_{\alpha'\zeta'}(\mathbb{k}')]. \tag{19}$$

In the case of electron-phonon scattering, $P_{\mathbb{k}\mathbb{k}'}$ is written as [3]

$$P_{\mathbb{k}\mathbb{k}'} = (2\pi/\hbar)\sum_{\vec{q}\nu}\left|g^{\vec{q}\nu}_{\mathbb{k}\mathbb{k}'}\right|^2 f(\varepsilon_{\mathbb{k}})(1-f(\varepsilon_{\mathbb{k}'})) \times [(n(\hbar\omega_{\vec{q}\nu},T_i)+1)\delta(\varepsilon_{\mathbb{k}}-\varepsilon_{\mathbb{k}'}-\hbar\omega_{\vec{q}\nu}) + n(\hbar\omega_{\vec{q}\nu},T_i)\delta(\varepsilon_{\mathbb{k}}-\varepsilon_{\mathbb{k}'}+\hbar\omega_{\vec{q}\nu})]. \quad (20)$$

Here $n(\hbar\omega_{\vec{q}\nu},T_i)$ is the Bose-Einstein distribution function, $\omega_{\vec{q}\nu}$ is phonon frequency, $g^{\vec{q}\nu}_{\mathbb{k}\mathbb{k}'}$ is an electron-phonon matrix element, which defines the probability of electron scattering from the initial state $\mathbb{k}$ into the final state $\mathbb{k}'$ after its interaction with a phonon with wave vector $\vec{q}$, polarization ν, and energy $\hbar\omega_{\vec{q}\nu}$ (the determination of $g^{\vec{q}\nu}_{\mathbb{k}\mathbb{k}'}$ for the FP-LMTO method can be found in Ref. [5]). The product of square brackets in Eq. (19) can be factorized,

$$[\chi_{\alpha\zeta}(\mathbb{k})-\chi_{\alpha\zeta}(\mathbb{k}')]\cdot[\chi_{\alpha'\zeta'}(\mathbb{k})-\chi_{\alpha'\zeta'}(\mathbb{k}')] = \frac{1}{4}\sum_{s,s'=\pm1}[F_\alpha(\mathbb{k})-sF_\alpha(\mathbb{k}')]\cdot[F_{\alpha'}(\mathbb{k})-s'F_{\alpha'}(\mathbb{k}')]\left[\frac{\eta_\zeta(\varepsilon)}{N(\varepsilon)\upsilon(\varepsilon)}+s\frac{\eta_\zeta(\varepsilon')}{N(\varepsilon')\upsilon(\varepsilon')}\right] \cdot\left[\frac{\eta_{\zeta'}(\varepsilon)}{N(\varepsilon)\upsilon(\varepsilon)}+s'\frac{\eta_{\zeta'}(\varepsilon')}{N(\varepsilon')\upsilon(\varepsilon')}\right]. \quad (21)$$

Here we can introduce, for convenience, a generalized electron-phonon spectral function

$$\alpha^2_{tr}F(s,s',\alpha,\alpha',\varepsilon,\varepsilon',\Omega) = \frac{1}{2N(\varepsilon)}\sum_{\vec{q}\nu}\delta(\Omega-\omega_{\vec{q}\nu})\sum_{\mathbb{k}\mathbb{k}'}\left|g^{\vec{q}\nu}_{\mathbb{k}\mathbb{k}'}\right|^2\delta(\varepsilon_{\mathbb{k}}-\varepsilon)\delta(\varepsilon_{\mathbb{k}'}-\varepsilon)\times[F_\alpha(\mathbb{k})-sF_\alpha(\mathbb{k}')]\cdot[F_{\alpha'}(\mathbb{k})-s'F_{\alpha'}(\mathbb{k}')] \quad (22)$$

and joint energy polynomials

$$J(s,s',\zeta,\zeta',\varepsilon,\varepsilon') = \frac{1}{4}\left[\frac{\eta_\zeta(\varepsilon)}{N(\varepsilon)\upsilon(\varepsilon)}+s\frac{\eta_\zeta(\varepsilon')}{N(\varepsilon')\upsilon(\varepsilon')}\right]\times\left[\frac{\eta_{\zeta'}(\varepsilon)}{N(\varepsilon)\upsilon(\varepsilon)}+s'\frac{\eta_{\zeta'}(\varepsilon')}{N(\varepsilon')\upsilon(\varepsilon')}\right]. \quad (23)$$

Then the expression for the scattering operator written in integral form becomes

$$Q_{\alpha\zeta,\alpha'\zeta'} = \frac{2\pi V}{\hbar k_B T_e}\int_0^\infty d\Omega\int_{-\infty}^\infty d\varepsilon\int_{-\infty}^\infty d\varepsilon'\sum_{s,s'=\pm1}\alpha^2_{tr}F(s,s',\alpha,\alpha',\varepsilon,\varepsilon',\Omega)N(\varepsilon)J(s,s',\zeta,\zeta',\varepsilon,\varepsilon')f(\varepsilon,T_e)(1-f(\varepsilon',T_e)) \times[(n(\hbar\Omega,T_i)+1)\delta(\varepsilon-\varepsilon'-\hbar\Omega)+n(\hbar\Omega,T_i)\delta(\varepsilon-\varepsilon'+\hbar\Omega)]. \quad (24)$$

Here V is the unit cell volume. In the static DFT methods such as FP-LMTO, the spectral function $\alpha^2_{tr}F$ is determined for specified fixed atomic positions.

Consider a case where the thermal and electric currents point in the x direction. Then, according to Eqs. (13), (16), and (17), if the off-diagonal elements of the scattering matrix $Q_{\alpha\zeta,\alpha'\zeta'}$ are small, the values of electrical resistivity (conductivity) and thermal conductivity are determined as [3]

$$\rho \approx \frac{1}{2e^2}Q_{x0,x0}, \quad (25)$$

$$\kappa_e \approx \frac{2\pi^2k_B^2T_e}{3}\left[(Q)^{-1}_{x1,x1}-\left|(Q^{-1})_{x0,x1}\right|^2Q_{x0,x0}\right], \quad (26)$$

$$\sigma = 1/\rho. \quad (27)$$

Expressions (24) and (26) were derived by Allen [3] and we rewrote them here for $T_e \neq T_i$. Formula (24) inspires some concerns regarding its practical implementation in the general case. Further, we will do some reasonable approximations, which make calculations a bit easier with almost no loss in accuracy. Remind here that for electron-phonon interaction, in accordance with the energy conservation law, ε' will take the value $\varepsilon+\hbar\Omega$ if the phonon is absorbed and $\varepsilon-\hbar\Omega$ if it is emitted. Since the scale of electron energy variation is much greater than that of phonon energies, we can write function (22) in the following way: $\alpha^2_{tr}F(s,s',\alpha,\alpha',\varepsilon,\varepsilon',\Omega)\approx\alpha^2_{tr}F(s,s',\alpha,\alpha',\varepsilon,\varepsilon,\Omega)\equiv\alpha^2_{tr}F(s,s',\alpha,\alpha',\varepsilon,\Omega)$ [35]. Similarly, assume that $N(\varepsilon)\upsilon(\varepsilon)$ and $N(\varepsilon')\upsilon(\varepsilon')$ are close to each other, then the product $N(\varepsilon)J$ in expression (24) can be written as

$$N(\varepsilon)J(s,s',\zeta,\zeta',\varepsilon,\varepsilon') = \frac{1}{4N(\varepsilon)\upsilon^2(\varepsilon)}[\eta_\zeta(\varepsilon)+s\eta_\zeta(\varepsilon')]\cdot[\eta_{\zeta'}(\varepsilon)+s'\eta_{\zeta'}(\varepsilon')]. \quad (28)$$

Figure 1 shows the dependence $N(\varepsilon)\upsilon^2(\varepsilon)$ we obtained in this paper for gold at different values of T_e and the cold lattice. It is seen that $N(\varepsilon)\upsilon^2(\varepsilon)$ is a smooth function oscillating at low T_e. But with the increasing temperature, its oscillations get much smaller and at $T_e \gtrsim 10$ kK the function becomes monotonic in the considered energy range.

Our calculations show that in expression (24), the terms with $s \neq s'$ can be omitted in summation over s, s' because of their negligible contribution to the determined quantity. With the above approximations and the fact that $\eta_0 = 1$, $\eta_1 = \sqrt{3}\varepsilon/(\pi k_B T_e)$ expressions for $Q_{x0,x0}$, $Q_{x1,x1}$, and $Q_{x0,x1}$

present in Eqs. (25) and (26) can be written as

$$Q_{x0,x0} = \frac{2\pi V}{\hbar k_B T_e} \int d\Omega \int d\varepsilon \frac{I_0(x,x,\varepsilon,\Omega)}{N(\varepsilon)\upsilon^2(\varepsilon)}, \tag{29}$$

$$I_0(x,x,\varepsilon,\Omega) = \alpha_{tr}^2 F(1,1,x,x,\varepsilon,\Omega) \int d\varepsilon' f(\varepsilon,T_e)(1-f(\varepsilon',T_e)) \times [(n(\hbar\Omega,T_i)+1)\delta(\varepsilon-\varepsilon'-\hbar\Omega) + n(\hbar\Omega,T_i)\delta(\varepsilon-\varepsilon'+\hbar\Omega)], \tag{30}$$

$$Q_{x1,x1} = \frac{6V}{\pi\hbar(k_B T_e)^3} \int d\Omega \int d\varepsilon \frac{I_1(x,x,\varepsilon,\Omega)}{N(\varepsilon)\upsilon^2(\varepsilon)}, \tag{31}$$

$$I_1(x,x,\varepsilon,\Omega) = \frac{1}{4}\sum_{s,s'=\pm1} \alpha_{tr}^2 F(s,s',x,x,\varepsilon,\Omega) \int d\varepsilon'(\varepsilon+s\varepsilon')(\varepsilon+s'\varepsilon') f(\varepsilon,T_e)(1-f(\varepsilon',T_e)) \times [(n(\hbar\Omega,T_i)+1)\delta(\varepsilon-\varepsilon'-\hbar\Omega) + n(\hbar\Omega,T_i)\delta(\varepsilon-\varepsilon'+\hbar\Omega)], \tag{32}$$

$$Q_{x0,x1} = \frac{\sqrt{3}V}{\hbar(k_B T_e)^2} \int d\Omega \int d\varepsilon \frac{I_{01}(x,x,\varepsilon,\Omega)}{N(\varepsilon)\upsilon^2(\varepsilon)}, \tag{33}$$

$$I_{01}(x,x,\varepsilon,\Omega) = \alpha_{tr}^2 F(1,1,x,x,\varepsilon,\Omega) \int d\varepsilon'(\varepsilon+\varepsilon') f(\varepsilon,T_e)(1-f(\varepsilon',T_e)) \times [(n(\hbar\Omega,T_i)+1)\delta(\varepsilon-\varepsilon'-\hbar\Omega) + n(\hbar\Omega,T_i)\delta(\varepsilon-\varepsilon'+\hbar\Omega)]. \tag{34}$$

The values of I_0, I_1, and I_{01} can easily be calculated by determining the function $\alpha_{tr}^2 F(s,s',x,x,\varepsilon,\Omega)$ and take into account that, according to energy conservation, integration over $d\varepsilon'$ can be eliminated for the processes of absorption $\varepsilon' = \varepsilon + \hbar\Omega$ and emission $\varepsilon' = \varepsilon - \hbar\Omega$ of phonons. With the known ε and $\hbar\Omega$, the value of ε', which gives a nonzero contribution to the integral is always determined. In our case it is necessary to calculate the spectral function within a certain range of interest, whose boundaries are defined by the Fermi-Dirac distribution.

For temperatures above Θ_D, we can apply the quasielastic approximation $\delta(\varepsilon-\varepsilon'\mp\hbar\Omega) \approx \delta(\varepsilon-\varepsilon')$, then the expressions for Q become yet simpler,

$$Q_{x0,x0} = \frac{2\pi V}{\hbar k_B T_e} \int d\Omega \int \frac{\alpha_{tr}^2 F(1,1,x,x,\varepsilon,\Omega) d\varepsilon}{N(\varepsilon)\upsilon^2(\varepsilon)} \times f(\varepsilon,T_e)(1-f(\varepsilon,T_e))[2n(\hbar\Omega,T_i)+1], \tag{35}$$

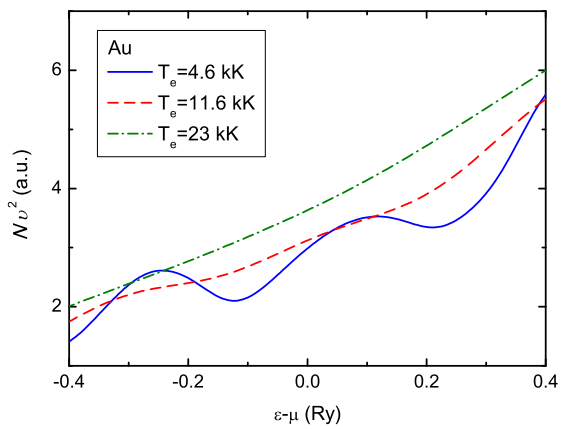

FIG. 1. The value of $N(\varepsilon)\upsilon^2(\varepsilon)$ vs energy at different electron temperatures T_e for gold.

$$Q_{x1,x1} = \frac{6V}{\pi\hbar(k_B T_e)^3} \int d\Omega \int \frac{\alpha_{tr}^2 F(1,1,x,x,\varepsilon,\Omega)\varepsilon^2 d\varepsilon}{N(\varepsilon)\upsilon^2(\varepsilon)} \times f(\varepsilon,T_e)(1-f(\varepsilon,T_e))[2n(\hbar\Omega,T_i)+1], \tag{36}$$

$$Q_{x0,x1} = \frac{2\sqrt{3}V}{\hbar(k_B T_e)^2} \int d\Omega \int \frac{\alpha_{tr}^2 F(1,1,x,x,\varepsilon,\Omega)\varepsilon d\varepsilon}{N(\varepsilon)\upsilon^2(\varepsilon)} \times f(\varepsilon,T_e)(1-f(\varepsilon,T_e))[2n(\hbar\Omega,T_i)+1]. \tag{37}$$

We have thus obtained the formulas to calculate the transport properties of metals in case of nonequilibrium heating, which will also be applicable in the equilibrium heating regime. Formulas (29)–(34) take into account all important effects, including the inelastic electron-phonon scattering. Having calculated from first principles the required quantities present in the formulas for the static lattice at different values of T_e, we can determine ρ (or σ) and κ_e as functions of (T_e, T_i) for any specified value of specific volume.

If switch to the equilibrium case $T_e = T_i \equiv T$ and consider only relatively low temperatures $T \lesssim 300$ K, we can neglect Fermi smearing, the dependence of $\alpha_{tr}^2 F$ on energy, and the thermoelectric term in κ_e [Eq. (26)]. As a result, formulas (29)–(32) become much simpler [3]. Taking into account that energy is measured relative to the Fermi energy $\mu = E_F$, we introduce the notations $\alpha_{tr}^2 F(1,\Omega) \equiv \alpha_{tr}^2 F(1,1,x,x,0,\Omega)$ and $\alpha_{tr}^2 F(-1,\Omega) \equiv \alpha_{tr}^2 F(-1,-1,x,x,0,\Omega)$, where the spectral function takes the form

$$\alpha_{tr}^2 F(\pm1,\Omega) = \frac{1}{2N(0)\upsilon^2(0)} \sum_{\vec{q}\nu} \delta(\Omega-\omega_{\vec{q}\nu}) \sum_{\mathbb{k}\mathbb{k}'} \left|g_{\mathbb{k}\mathbb{k}'}^{\vec{q}\nu}\right|^2 (\upsilon_x(\mathbb{k}) \mp \upsilon_x(\mathbb{k}'))^2 \delta(\varepsilon_{\mathbb{k}})\delta(\varepsilon_{\mathbb{k}'}). \tag{38}$$

Then, after appropriate transformation of energy integrals in Eqs. (29)–(32), formulas for electrical resistivity and thermal conductivity can be written as [3,4]

$$\rho = \frac{2\pi V k_B T}{e^2 \hbar N(0) v^2(0)} \int_0^\infty \frac{d\Omega}{\Omega} \frac{x^2}{\sinh^2(x)} \alpha_{tr}^2 F(1,\Omega), \quad (39)$$

$$\frac{1}{\kappa_e} = \frac{6V}{\pi \hbar k_B N(0) v^2(0)} \int_0^\infty \frac{d\Omega}{\Omega} \frac{x^2}{\sinh^2(x)} \times \left[\alpha_{tr}^2 F(1,\Omega) \left(1 + \frac{x^2}{\pi^2}\right) + \frac{3x^2}{\pi^2} \alpha_{tr}^2 F(-1,\Omega) \right]. \quad (40)$$

where $x = \Omega/(2k_B T)$. It should be noted here that at high temperatures formula (39) gives a linear dependence of ρ on T, and κ_e calculated from (40) will be approaching a constant value [4]. Below these formulas are used for comparison with more general expressions (25), (26), (29)–(34) in the equilibrium heating regime.

B. Parameters of *ab initio* calculations

To calculate the transport properties of copper, silver, gold, and palladium from first principles, we used in this paper the all-electron full-potential linear muffin-tin orbital method [36]. Within density functional theory, the FP-LMTO method calculates the energy and the electron density distribution at various electron temperatures and material densities. The phonon spectra and spectral electron-phonon functions for the above metals were calculated with linear response theory implemented in the FP-LMTO code [5,36]. The high accuracy of our *ab initio* calculations was attained through the careful choice of FP-LMTO parameters. Since we have already studied some of the metals [35,37], calculation parameters were largely the same as used earlier. First of all, this concerns the choice of the exchange-correlation (XC) functional. It was chosen so as to allow the best possible description of ground-state properties and phonon spectra for the metals of interest. These were the functional from Ref. [38] with gradient corrections [39] for copper and palladium, the local XC functional [40] for gold, and the PBEsol [41] XC for silver. The valence electrons in calculations were $3p$, $3d$, $4s$ for Cu; $4p$, $4d$, $5s$ for Ag; $5p$, $5d$, $6s$ for Au; and $4d$, $5s$ for Pd. These were quite sufficient because calculations were done for the densities of metals close to those at ambient conditions and electron temperatures $\lesssim 20$ kK.

Integration over the Brillouin zone was done with the improved tetrahedron method [42]. The mesh in $\vec{k}$ space was taken to be $40 \times 40 \times 40$ for all metals under consideration. As shown by calculations, such dense meshes are necessary for accurate determination of the electron-phonon spectral function. A mesh of $10 \times 10 \times 10$ appeared sufficient for phonon spectrum integration over $\vec{q}$ points. For more details about meshes, see the first part of the Appendix. The cutoff energy in the representation of basis functions by a set of plane waves in the interstitial region was taken to be 1000 eV. The set of basis functions was limited to the orbital moment $l_{\max}^b = 5$. The spherical harmonic expansion of the charge density and the potential was done to the moment $l_{\max}^w = 7$. The FP-LMTO parameters, such as linearization energies, tail energies, and others were selected with an approach similar to that described in Ref. [43].

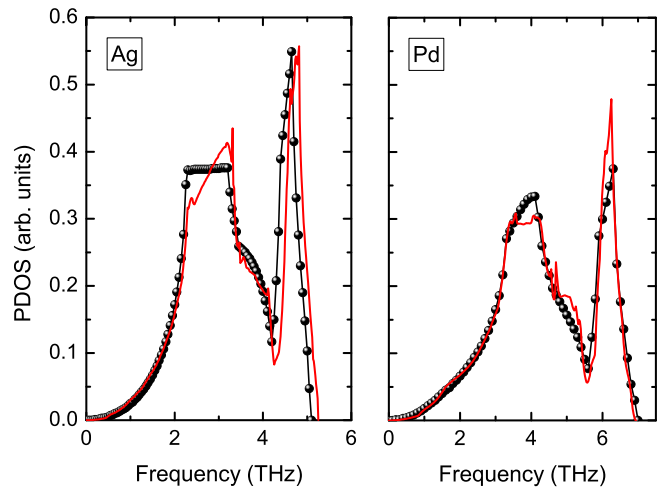

FIG. 2. Phonon spectra of silver and palladium at experimental equilibrium specific volume. The red lines show the calculation done in this paper at zero temperature, and the circles connected by lines show experimental results at room temperature [44].

With the thoroughly adjusted parameters of the FP-LMTO method we succeeded to reproduce the experimental equilibrium specific volume V_0 to better than 2%. The accuracy of phonon spectra calculated for Cu and Au was demonstrated earlier in paper [35]. Therefore, here we only provide comparison for silver and palladium as shown in Fig. 2. The calculated phonon densities of state (PDOS) are seen to agree well with experiment. Such a good agreement gives us a hope that the function $\alpha_{tr}^2 F$ will also be reproduced well in the calculations presented below.

III. RESULTS

First consider results we obtained in our calculation of transport properties for Cu, Ag, Au, and Pd in the equilibrium heating regime. Since we are dealing with cubic crystals, only the x component of Q needs to be calculated in order to obtain ρ and κ_e. For convenience, let us use EF to refer to calculations by formulas (25), (26), and (29)–(34) as the most accurate, QE for calculations in quasielastic approximation by formulas (25), (26), and (35)–(37), and AF for calculations by approximations (38)–(40).

Figures 3–6 present the temperature dependencies of electrical resistivity and thermal conductivity calculated in this paper in different approximations in comparison with available experimental data. The light green curves show the EF calculations, and the blue ones show the AF calculations along the isochore of the equilibrium specific volume V_0. In addition, QE results (green-dashed line) for copper and gold at $V = V_0$ are provided. Since experimental results are measured along an isobar rather than an isochore, we also did calculations where volume was changed with the increasing temperature. That was done in a simple form using experimental equations of state for Cu, Ag, and Au [52], and precise crystallographic data for Pd [53]. The band structure computations were done for each specific volume considered. The red line in Figs. 3–6 shows EF results in the case of volume variation.

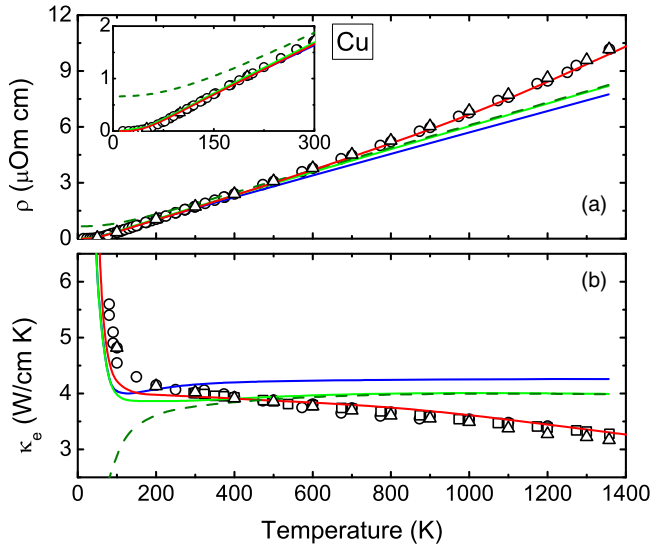

FIG. 3. Electric resistivity (a) and thermal conductivity (b) of copper vs temperature. Experimental data: circles [45,46], triangles [47], and squares [48]. Computational results: the solid green and red lines are EF calculations for $V = V_0$ and with account for volume variation, respectively (see the text); the dashed green line is QE calculations for $V = V_0$, and the solid-blue line is AF calculations also for $V = V_0$. The inset shows the region of low T for resistivity ρ.

As seen from Figs. 3–6, the utilization of the EF formulas with account for volume variation helps catch the correct shape of the curves $\rho(T)$ and $\kappa_e(T)$, and get results, which agree well with experiment in a wide range of temperatures as for Cu, Ag, and Au, so for Pd. A specific feature is seen for palladium. Unlike the other metals, the changing volume

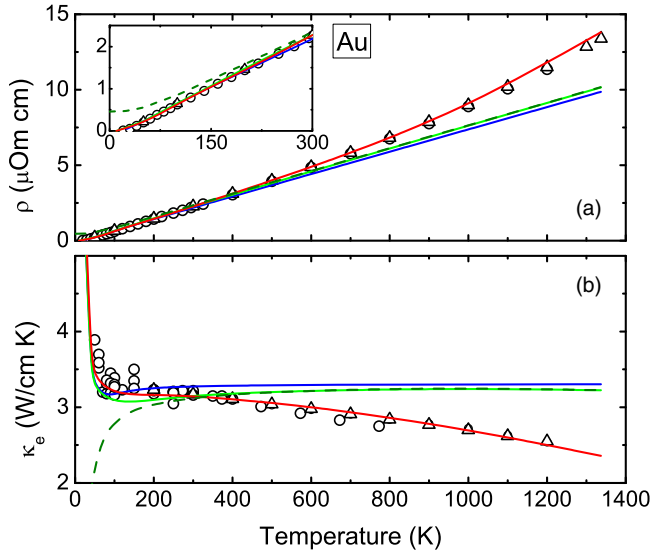

FIG. 4. Electrical resistivity (A) and thermal conductivity (B) of gold versus temperature from experiments (circles [45,46] and triangles [47]) and calculations (see the legend of Fig. 3 for details). The inset shows the region of low T for ρ.

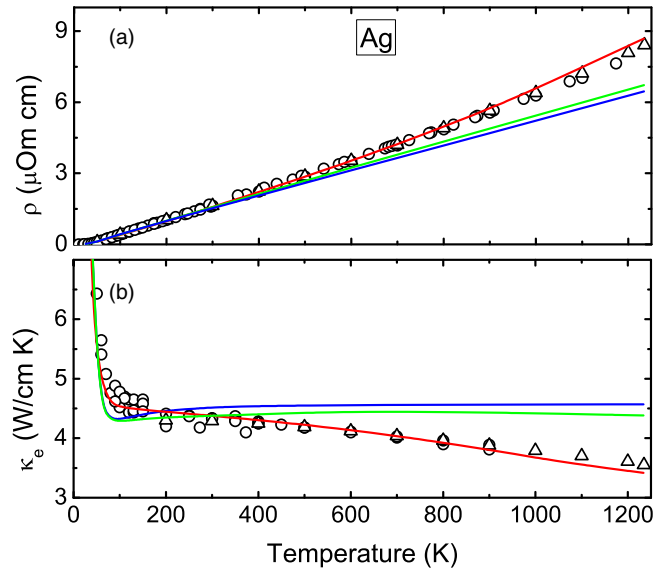

FIG. 5. Electrical resistivity (a) and thermal conductivity (b) of silver vs temperature from experiments (circles [45,46] and triangles [47]) and calculations (see the legend of Fig. 3 for details)

weakly influences $\rho(T)$, while for $\kappa_e(T)$, the growth of V at $T > 600$ K becomes important.

For Cu, Ag, and Au, the AF results agree rather well with the EF calculations for isochoric heating, i.e., account for Fermi smearing and the energy dependence of spectral function $\alpha^2_{tr}F$ is of a small effect (<5%). However, as seen from Fig. 6, the situation markedly differs for palladium. With the simplified AF expressions we failed to reproduce both the slowing growth of electrical resistivity and the increase of κ_e above room temperature, as observed in experiment. In

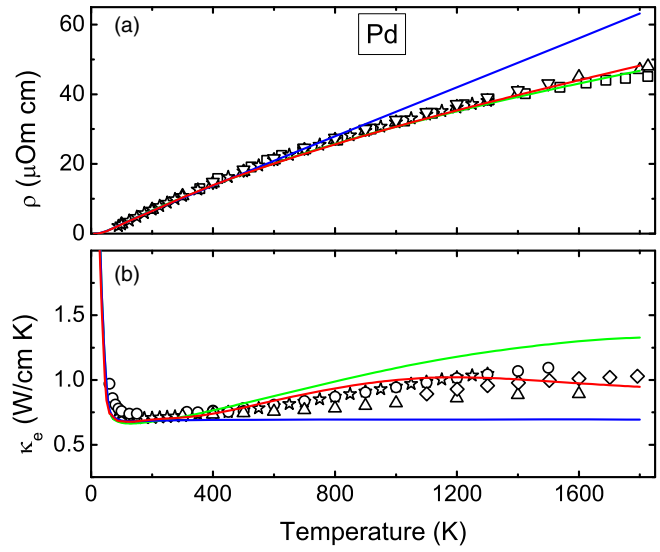

FIG. 6. Electrical resistivity (a) and thermal conductivity (b) of palladium vs temperature. Experimental data: circles [45,46], triangles [47], turned triangles [49], squares [50], pentagons [51], diamonds [55]). The lines are computed results (see the legend of Fig. 3 for details).

the EF calculations for Pd at high T, $\rho(T)$ is not linear and $\kappa_e(T)$ does not become constant at high temperatures. The differences in calculations for the considered metals come from a significant difference in their band structure [54]. Bands with d electrons in palladium cross the Fermi level in such a way that the electron density of states in the near vicinity of E_F significantly changes in contrast to the other metals where it remains almost constant. So, on the Fermi level, the electron density of states in Pd is more than eight times higher than in the other metals. The changes induced by the increasing temperature in the electron density of states of Pd near the Fermi level give a greater contribution to the determined quantities, and the inclusion of Fermi smearing and the energy dependence of spectral function helps correctly account for the effect of these changes.

It is clearly seen from Figs. 3 and 4 that at T above the Debye temperature ($\Theta_D \approx 340$ K for Cu and $\approx$165 K for Au), the QE results give good agreement with calculations by the more accurate formulas (i.e., the EF results) and above these temperatures one can safely use quasielastic expressions (35)–(37) to calculate ρ and κ_e. It is also seen that at low T, the accuracy of the quasielastic approximation strongly decreases and the results begin to differ significantly from the most accurate solution. It is of critical importance here to include inelastic scattering.

Now consider the nonequilibrium heating regime of the metals under study. Here gold is the most studied material. As mentioned above, in the experiment reported in Ref. [23], the authors succeeded to measure the temporal evolution of DC electrical conductivity σ in free-standing thin (30 nm) gold foils irradiated by ultraviolet laser pulses of duration $\tau_p =$ 150 fs. When such ultrashort pulses interact with matter, they are almost immediately absorbed by the electron subsystem whose temperature sharply increases while the ions remain relatively cold. With time, the temperatures equalize due to electron-phonon interaction. Since according to estimates, the temperatures achieved in the experiment are noticeably lower than the Fermi temperature, the excited electrons are assumed to recombine fast and their distribution will be close to the Fermi-Dirac one [23].

In order to describe such an experiment we need to know how the electron and lattice temperatures vary with time. We limited ourselves to a simulation time of 20 ps because experiments [23,33] show that the foil that absorbed the appropriate amount of energy, viz, 0.89 MJ/kg [23], can be considered completely molten after that time. Electron and ion temperatures can be found with a two-temperature model [26,27]. Ion thermal conductivity can be neglected because in this case it is much lower than electron thermal conductivity. Since the irradiated foil is quite thin, we will also neglect the electron thermal conductivity since such targets are uniformly heated due to energy transfer by ballistic electrons and electron thermal diffusion over times of the order of τ_p [23]. The equations to be solved are

$$C_e(T_e)\frac{\partial T_e}{\partial t} = -(T_e - T_i)G(T_e) + S(t), \tag{41}$$

$$C_i(T_i)\frac{\partial T_i}{\partial t} = (T_e - T_i)G(T_e). \tag{42}$$

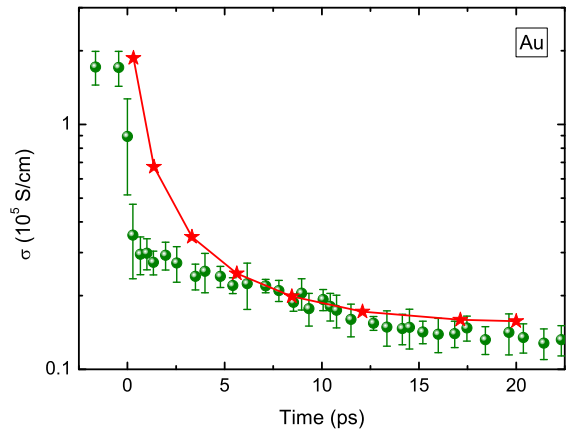

FIG. 7. The time dependence of DC conductivity for gold irradiated by ultrashort laser pulses ($\tau_p = 150$ fs). Circles are experimental data from paper [23] and stars connected by a line are calculation results.

Here C_e and C_i are electron and lattice specific heats, respectively, $S(t)$ is a Gaussian-shaped source term [18], and G is the electron-phonon coupling factor dependent on T_e. The way of calculation from first principles and the values of the above parameters for gold and copper can be found in Ref. [35] and we will not go into these details here. The accuracy of those calculations is also discussed in that paper. For silver and palladium, the calculated factors $G(T_e)$ are presented in the Appendix. Knowing the values of T_e and T_i for each time, one can calculate electrical conductivity using formulas (25), (27), (29), and (30).

Figure 7 shows calculated results obtained in this work in comparison with experiment [23]. It is seen that σ dramatically changes with time; its value drops very fast after irradiation. Calculated values agree quite well with the experimental behavior of electrical conductivity, and the agreement improves as time increases. It is quite possible that for better agreement between the experimental and calculated results at $t < 4$ ps, it will be necessary to take into account the electron-electron scattering in the calculation of σ, as noted in Ref. [23], since for these times the electron temperature is rather high, above 12 kK, while the ion temperature is still low. On whole, the results obtained with formulas (25), (27), (29), and (30) demonstrate rather high accuracy.

Further, consider how electrical and thermal conductivities calculated by EF formulas (25)–(27) and (29)–(34) vary with T_e for several lattice temperatures T_i. The calculations were done for volume corresponding to the experimental specific volume V_0 under ambient conditions. Figures 8–11 present their results for the considered metals. Here we do not provide results obtained with the quasielastic approximation because they agree very well with the more accurate EF calculations in this temperature range. Also note that calculations at a lattice temperature $T_i = 2000$ K, which is above the known melting point for these metals can be of sense since, as stated in Refs. [56,57], there exists a possibility for lattice to become strongly overheated because the interionic potential strongly changes after the heating of the electron subsystem by the ultrashort pulse. So, for example, *ab initio* calculations [57]

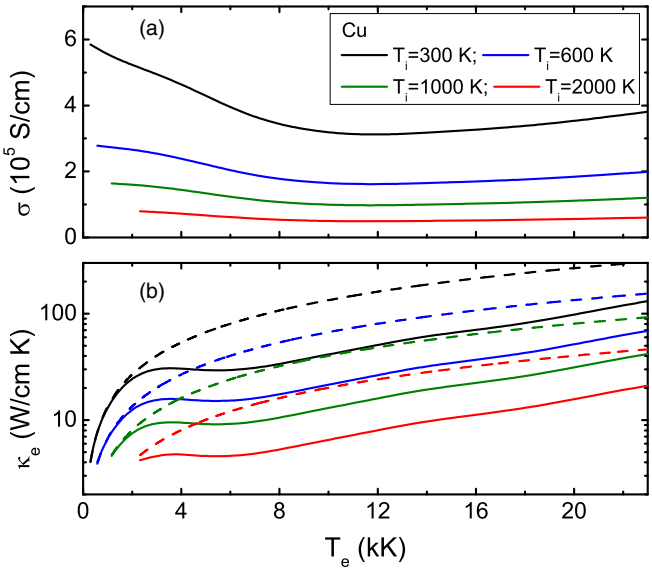

FIG. 8. Calculated DC conductivity (a) and thermal conductivity (b) of copper vs T_e for different lattice temperatures T_i: EF calculation results (solid lines) and κ_e calculations by semi-empirical formula (43) (dashed lines).

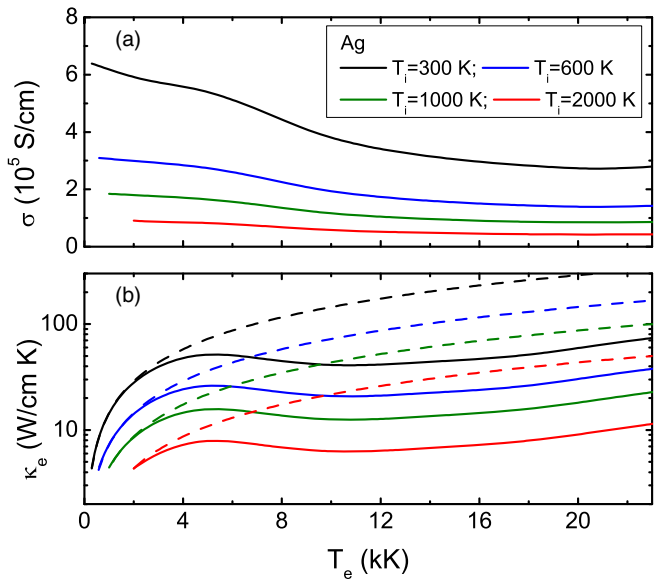

FIG. 10. Calculated DC conductivity (a) and thermal conductivity (b) of silver vs T_e at different lattice temperatures T_i: EF calculation results (solid lines) and κ_e calculations by semi-empiric formula (43) (dashed lines).

show vacancy formation enthalpy in the gold lattice to become more than three times higher at $T_e = 23$ kK than at room temperature. Surely, this must be of effect on the melting temperature. There are various estimations of the possible change in the melting temperature of metals as a result of its nonequilibrium heating [35,58,59]. All of them based on the Lindemann criterion, which is an approximate approach for calculation of the melting temperature. For more accurate calculations, more sophisticated methods such as *ab initio* molecular dynamics may be needed.

First, look at electrical conductivity. As seen from Figs. 8–10(a), the conductivity of Cu, Ag, and Au for a given T_i first decreases with the growing T_e and then begins to slowly increase (in Au this happens above 23 kK). For palladium, the situation is somewhat different: At a given T_i, $\sigma(T_e)$ increases at temperatures $\lesssim 8$ kK and at higher T_e firstly slightly decreases and then grows a little bit. Such a behavior is due to the previously mentioned feature of the band structure of this metal. With the increasing lattice temperature the value of σ

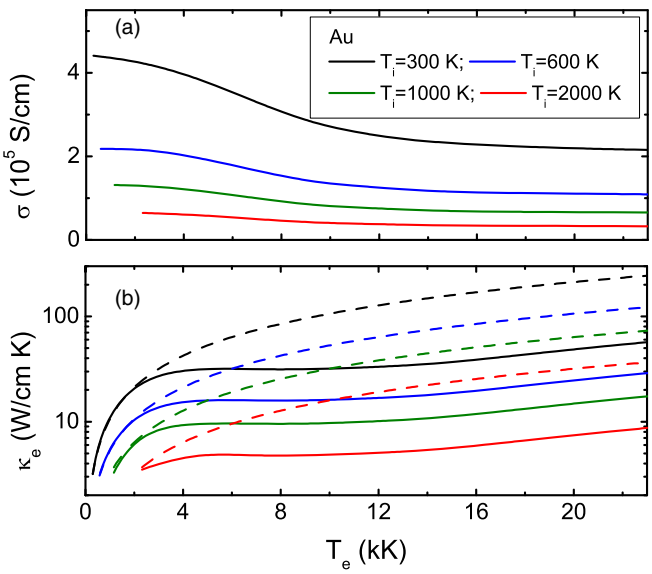

FIG. 9. Calculated DC conductivity (a) and thermal conductivity (b) of gold vs T_e for different lattice temperatures T_i: EF calculation results (solid lines) and κ_e calculations by semi-empiric formula (43) (dashed lines).

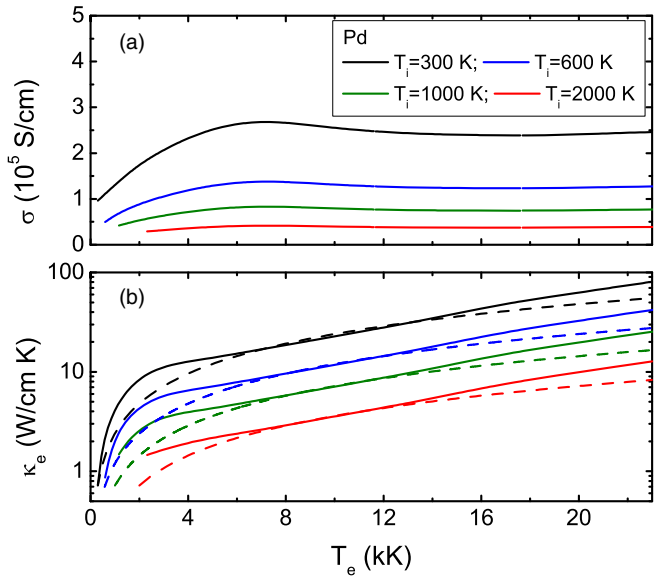

FIG. 11. Calculated DC conductivity (a) and thermal conductivity (b) of palladium vs T_e at different lattice temperatures T_i: EF calculation results (solid lines) and κ_e calculations by semi-empiric formula (43) (dashed lines).

sharply decreases as for Cu, Ag, and Au, so for palladium. Also seen, as T_i elevates, electrical conductivity becomes practically independent of T_e, which agrees well with calculations by the Kubo-Greenwood formula for some other metals [60].

Let us consider thermal conductivity [Figs. 8–11(b)]. The dashed lines additionally drawn in Figs. 8–11(b) show results obtained with the formula, which is often used in two-temperature calculations [27,61],

$$\kappa_e = K_0 \frac{T_e}{T_i}, \tag{43}$$

where K_0 is a constant that is adjusted through comparison with low-temperature experiment at $T_e = T_i$. In formula (43), we neglect the term associated with electron-electron scattering, which is not considered in this paper. As stated in Refs. [27,61,62], this dependence works well for quite low temperatures. It is however difficult to determine the range of its applicability for each specific element from general consideration. Besides formula (43) known from the literature, there is the more general wide-range formula [27]

$$\kappa_e = C \cdot \frac{(\theta^2 + 0.16)^{5/4}(\theta^2 + 0.44) \cdot \theta}{(\theta^2 + 0.092)^{1/2}(\theta^2 + b \cdot \theta_i)}, \tag{44}$$

where $\theta = k_B T_e / E_F$, $\theta_i = k_B T_i / E_F$, and C and b are adjustable constants. Unlike (43), expression (44) tends to a dependence typical of nondegenerate plasma, $\kappa_e \sim T_e^{5/2}$, in the limit of high T_e, while in the limit of low temperatures its functional form coincides with formula (43).

On whole, the dependencies $\kappa_e(T_e)$ calculated by the EF formulas show a tendency to increase with the growing T_e [Figs. 8–11(b)]. However for Cu, Ag, and Au, the interval where κ_e initially shows a quite sharp increase is followed by a small interval where it slightly decreases. Like in the case of electrical conductivity, the increase of T_i results in a strong decrease of thermal conductivity. If compare the EF results with calculations by formula (43), then for Cu, Ag, and Au, a clear tendency is seen to overestimate κ_e in the semi-empirical approach at temperatures above 2 kK. Below these temperatures the results of two calculations agree very well. At $T_e = 10$ kK, the two types of calculations differ by more than three times. The dependence $\kappa_e(T_e)$ from EF calculation noticeably departs from linear as T_e increases. Possibly, it is caused by the effect of the energy dependence of the transport function $\alpha_{tr}^2 F$ at high temperatures. Note that in the temperature range under consideration, the effect of the thermoelectric term in Eq. (26) is less than 10% for Cu, Ag, and Au.

The effect of difference in the band structure on thermal conductivity can be seen from comparison between results for Cu, Ag, and Au and results for palladium [Fig. 11(b)]. Firstly, the $\kappa_e(T_e)$ curves for Pd do not have the temperature interval where thermal conductivity decreases. Secondly, formula (43) here underestimates κ_e at rather low ($T_e < 7$ kK) and high ($T_e > 14$ kK) temperatures. Even at relatively low temperatures where T_e and T_i are still close to each other, the results obtained by the two types of calculations differ markedly, especially for $T_i > 600$ K. This is due to the fact that the dependence of the thermal conductivity $\kappa_e(T)$ (for $T_e = T_i$) of palladium along the isochore does not reach a constant value with the increasing temperature, but increases, which, of course, is not taken into account by formula (43). Expression (43) will give incorrect results for all metals for which such behavior occurs. Consequently, heat diffusion from the surface into deeper parts of the irradiated target will be underestimated. Thus, in the case of palladium, the influence of the dependence of $\alpha_{tr}^2 F$ on energy manifests itself already at rather low temperatures (below the melting point). The effect of the thermoelectric term on the thermal conductivity of Pd is also much higher. Its correction may reach 50% at $T_e > 10$ kK.

IV. CONCLUSIONS

In this paper, on the basis of the method proposed by Allen [3] to solving the Boltzmann equation, formulas were derived to calculate the electron transport properties of solid-state metals in the nonequilibrium heating regime with account for electron-phonon interaction. These formulas are applicable within a rather wide range of electron temperatures (a few eV) and can be used in cases where electron and lattice temperatures strongly differ. They also give good results in case of equilibrium heating for T from a few tens of kelvins up to melting. The expressions work most effectively in calculations where the Fermi smearing of the electron distribution function and the energy dependence of the electron-phonon spectral function need to be taken into account. We also propose formulas to calculate the transport properties in a more simple quasielastic approximation and show it to be accurate for T above Θ_D. In contrast to the frequently used Kubo-Greenwood formula, in the proposed approach no averaging over ionic configurations is required for a given density of matter, but only one calculation of the phonon spectrum and the electron-phonon spectral function is sufficient. Also, since the linear response method was used for phonon spectrum calculations, there is no need to consider a supercell for simulation, it is quite enough to take only the unit cell of the crystal.

Our approach is implemented within the first-principles all-electron FP-LMTO method. Calculations performed in this work gave the temperature dependencies of electrical resistivity (DC conductivity) and thermal conductivity of Cu, Ag, Au, and Pd both for equal and different electron and lattice temperatures. Obtained results agree well with available experimental data. So, for $T_e = T_i$ they reproduce well the slowing growth of electrical resistivity and the increase of thermal conductivity in palladium above room temperature. Results for the nonequilibrium heating of gold well reproduce the temporal evolution of its DC electrical conductivity observed in modern laser experiments [23]. It is also shown that in case of Cu, Ag, and Au, the widely-used semi-empiric dependence $\kappa_e \sim T_e$ works well only at relatively low temperatures ($\lesssim 2$ kK) and overestimates thermal conductivity at higher temperatures. For palladium, κ_e is underestimated already at relatively low temperatures. These factors should be taken into account in the simulation of ultrashort laser interaction with matter and the construction of new wide-range analytical thermal conductivity models for metals.

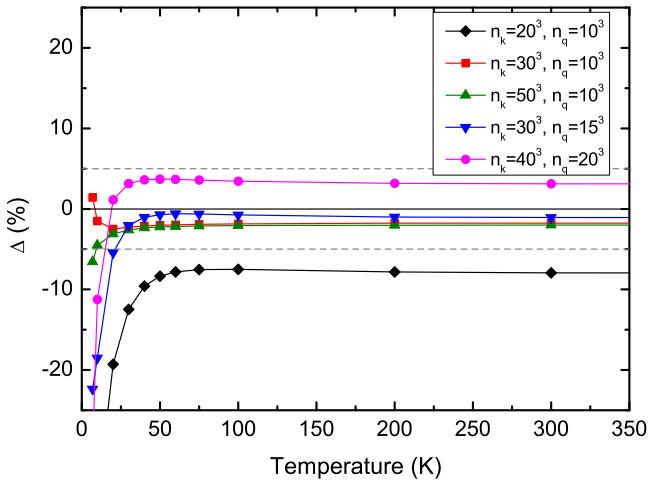

FIG. 12. Relative deviation of thermal conductivity of palladium versus temperature for different $\vec{k}$ and $\vec{q}$ meshes (normal specific volume, equilibrium heating). The data are presented relative to the $40 \times 40 \times 40$ $\vec{k}$ mesh and $10 \times 10 \times 10$ $\vec{q}$ mesh used for calculations in this paper.

ACKNOWLEDGMENTS

The author thanks Dr. A. A. Ovechkin and Dr. P. R. Levashov for the helpful discussion of the approach presented and the obtained results.

APPENDIX

1. Selection of the $\vec{k}$ and $\vec{q}$ meshes

Figure 12 presents the calculated relative deviations of palladium thermal conductivity versus T under equilibrium heating for different $\vec{k}$ and $\vec{q}$ meshes. They are given relative to the calculation of $40 \times 40 \times 40$ $\vec{k}$ mesh and $10 \times 10 \times 10$ $\vec{q}$ mesh. The equidistant meshes of $\vec{k}$ and $\vec{q}$ vectors are consistent, i.e., any point of the $\vec{q}$ mesh is a point of the $\vec{k}$ mesh. Calculations were done with no interpolation procedure from less dense meshes to more dense ones. It is seen that at temperatures from 30 K and above, all calculations except for, the $20 \times 20 \times 20$ $\vec{k}$ mesh and $10 \times 10 \times 10$ $\vec{q}$ mesh are accurate within 5%. This accuracy is quite sufficient since different experiments give a scattering of 5–10% on κ. At temperatures below 30 K, better accuracy requires denser meshes, but for these temperatures it is also necessary to consider the electron-electron interaction that begins to dominate.

TABLE I. The electron-phonon coupling factors, G (10^{17} W/m^{3}K), at different electron temperatures for Ag and Pd.

T_e (kK)	G_{Ag}	G_{Pd}
0.3	0.264	9.63
2.5	0.273	7.43
5.0	0.288	6.08
7.5	0.427	5.46
10	0.623	5.04
12.5	0.830	4.72
15	1.020	4.48
17.5	1.190	4.32
20	1.350	4.22
22.5	1.520	4.16

2. The electron-phonon coupling factors of Ag and Pd

Table I presents calculated electron-phonon coupling factors for silver and palladium. The method of their calculation is described in Ref. [35]. The coefficients are determined for the static fcc lattice.

[1] F. J. Pinski, P. B. Allen, W. H. Butler, Electron-phonon contribution to electrical resistivity and superconducting "*p*-wave" transition temperature of Pd, Phys. Rev. Lett. **41**, 431 (1978).

[2] P. B. Allen, Fermi-surface harmonics: A general method for nonspherical problems. Application to Boltzmann and Eliashberg equations, Phys. Rev. B **13**, 1416 (1976).

[3] P. B. Allen, New method for solving Boltzmann's equation for electrons in metals, Phys. Rev. B **17**, 3725 (1978).

[4] F. J. Pinski, P. B. Allen, W. H. Butler, Calculated electrical and thermal resistivities of Nb and Pd, Phys. Rev. B **23**, 5080 (1981).

[5] S. Y. Savrasov, D. Y. Savrasov, Electron-phonon interactions and related physical properties of metals from linear-response theory, Phys. Rev. B **54**, 16487 (1996).

[6] R. Bauer, A. Schmid, P. Pavone, and D. Strauch, Electron-phonon coupling in the metallic elements Al, Au, Na, and Nb: A first-principles study, Phys. Rev. B **57**, 11276 (1998).

[7] B. Xu, M. J. Verstraete, First Principles Explanation of the Positive Seebeck Coefficient of Lithium, Phys. Rev. Lett. **112**, 196603 (2014).

[8] B. Xu, M. Di Gennaro, M. J. Verstraete, Thermoelectric properties of elemental metals from first-principles electron-phonon coupling, Phys. Rev. B **102**, 155128 (2020).

[9] W. Li, Electrical transport limited by electron-phonon coupling from Boltzmann transport equation: An *ab initio* study of Si, Al, and MoS_2, Phys. Rev. B **92**, 075405 (2015).

[10] G. Pizzi, D. Volja, B. Kozinsky, M. Fornari, N. Marzari, BoltzWann: A code for the evaluation of thermoelectric and electronic transport properties with a maximally-localized Wannier functions basis, Comput. Phys. Commun. **185**, 422 (2014).

[11] G. K. H. Madsen, J. Carrete, M. J. Verstraete, BoltzTraP2, a program for interpolating band structures and calculating semi-classical transport coefficients, Comput. Phys. Commun. **231**, 140 (2018).

[12] S. Poncé, W. Li, S. Reichardt, F. Giustino, First-principles calculations of charge carrier mobility and conductivity in bulk semiconductors and two-dimensional materials, Rep. Prog. Phys. **83**, 036501 (2020).

[13] S. Li, Z. Tong, X. Zhang, H. Bao, Thermal conductivity and Lorenz ratio of metals at intermediate temperatures with mode-level first-principles analysis, Phys. Rev. B **102**, 174306 (2020).

[14] J. Sólyom, *Fundamentals of the Physics of Solids* (Springer, Berlin, 2009).

[15] M. Pozzo, C. Davies, D. Gubbins, D. Alfè, Thermal and electrical conductivity of iron at earth's core conditions, Nature (London) **485**, 355 (2012).

[16] H. Gomi, T. Yoshino, Impurity Resistivity of fcc and hcp Fe-based alloys: Thermal stratification at the top of the core of super-earths, Front. Earth Sci. **6**, 217 (2018).

[17] H. Gomi, T. Yoshino, Resistivity, Seebeck coefficient, and thermal conductivity of platinum at high pressure and temperature, Phys. Rev. B **100**, 214302 (2019).

[18] S. Mazevet, J. Clérouin, V. Recoules, P. M. Anglade, G. Zerah, *Ab-Initio* Simulations of the Optical Properties of Warm Dense Gold, Phys. Rev. Lett. **95**, 085002 (2005).

[19] A. Kietzmann, R. Redmer, M. P. Desjarlais, T. R. Mattsson, Complex Behavior of Fluid Lithium under Extreme Conditions, Phys. Rev. Lett. **101**, 070401 (2008).

[20] D. V. Knyazev, P. R. Levashov, *Ab initio* calculation of transport and optical properties of aluminum: Influence of simulation parameters, Comput. Mater. Sci. **79**, 817 (2013).

[21] D. V. Knyazev, P. R. Levashov, Thermodynamic, transport, and optical properties of dense silver plasma calculated using the GreeKuP code, Contrib. Plasma Phys. **59**, 345 (2019).

[22] Z. Chen, B. Holst, S. E. Kirkwood, V. Sametoglu, M. Reid, Y. Y. Tsui, V. Recoules, and A. Ng, Evolution of ac Conductivity in Nonequilibrium Warm Dense Gold, Phys. Rev. Lett. **110**, 135001 (2013).

[23] Z. Chen, C. B. Curry, R. Zhang, F. Treffert, N. Stojanovic, S. Toleikis, R. Pan, M. Gauthier, E. Zapolnova, L. E. Seipp *et al.*, Ultrafast multi-cycle terahertz measurements of the electrical conductivity in strongly excited solids, Nat. Commun. **12**, 1638 (2021).

[24] Y. T. Lee, R. M. More, An electron conductivity model for dense plasmas, Phys. Fluids **27**, 1273 (1984).

[25] A. Ng, P. Sterne, S. Hansen, V. Recoules, Z. Chen, Y. Y. Tsui, B. Wilson, DC conductivity of two-temperature warm dense gold, Phys. Rev. E **94**, 033213 (2016).

[26] S. I. Anisimov, B. L. Kapeliovich, and T. L. Perel'man, Electron emission from metal surfaces exposed to ultrashort laser pulses, Zh. Eksp. Teor. Fiz. **66**, 776 (1974) [Sov. Phys. JETP **39**, 375 (1974)].

[27] S. I. Anisimov, B. Rethfeld, On the theory of ultrashort laser pulse interaction with a metal, Proc. SPIE **3093**, 192 (1997).

[28] M. E. Povarnitsyn, N. E. Andreev, E. M. Apfelbaum, T. E. Itina, K. V. Khishchenko, O. F. Kostenko, P. R. Levashov, M. E. Veysman, A wide-range model for simulation of pump-probe experiments with metals, Appl. Surf. Sci. **258**, 9480 (2012).

[29] R. Li, O. A. Ashour, J. Chen, H. E. Elsayed-Ali, P. M. Rentzepis, Femtosecond laser induced structural dynamics and melting of Cu (111) single crystal. An ultrafast time-resolved x-ray diffraction study, J. Appl. Phys. **121**, 055102 (2017).

[30] Y. V. Petrov, N. A. Inogamov, K. P. Migdal, Thermal conductivity and the electron-ion heat transfer coefficient in condensed media with a strongly excited electron subsystem, JETP Lett. **97**, 20 (2013).

[31] A. A. Ovechkin, P. A. Loboda, A. L. Falkov, Transport and dielectric properties of dense ionized matter from the average-atom RESEOS model, High Energy Density Phys. **20**, 38 (2016).

[32] Yu. V. Petrov, N. A. Inogamov, V. A. Khokhlov, K. P. Migdal, Electron thermal conductivity of nickel and aluminum in solid and liquid phases in two-temperature states, J. Phys.: Conf. Ser. **1787**, 012025 (2021).

[33] M. Z. Mo, Z. Chen, R. K. Li, M. Dunning, B. B. L. Witte, J. K. Baldwin, L. B. Fletcher, J. B. Kim, A. Ng, R. Redmer *et al.*, Heterogeneous to homogeneous melting transition visualized with ultrafast electron diffraction, Science **360**, 1451 (2018).

[34] P. B. Allen, Boltzmann Theory and Resistivity of Metals, in *Quantum Theory of Real Materials* (Kluwer, Boston, 1996), chap. 17.

[35] N. A. Smirnov, Copper, gold, and platinum under femtosecond irradiation: Results of first-principles calculations, Phys. Rev. B **101**, 094103 (2020).

[36] S. Yu. Savrasov, Linear-response theory and lattice dynamics: A muffin-tin-orbital approach, Phys. Rev. B **54**, 16470 (1996).

[37] N. A. Smirnov, Relative stability of Cu, Ag, and Pt at high pressures and temperatures from ab initio calculations, Phys. Rev. B **103**, 064107 (2021).

[38] O. Gunnarsson, B. I. Lundqvist, Exchange and correlation in atoms, molecules, and solids by spin-density-functional formalism, Phys. Rev. B **13**, 4274 (1976).

[39] J. P. Perdew, J. A. Chevary, S. H. Vosko, K. A. Jackson, M. R. Pederson, D. L. Singh, C. Fiolhais, Atoms, molecules, solids, and surfaces: Applications of the generalized gradient approximation for exchange and correlation, Phys. Rev. B **46**, 6671 (1992).

[40] J. P. Perdew, *Electronic Structure of Solids'91* (Akademie, Berlin, 1991) p. 11.

[41] J. P. Perdew, A. Ruzsinszky, G. I. Csonka, O. A. Vydrov, G. E. Scuseria, L. A. Constantin, X. Zhou, K. Burke, Restoring the Density-Gradient Expansion for Exchange in Solids and Surfaces, Phys. Rev. Lett. **100**, 136406 (2008).

[42] P. Blöchl, O. Jepsen, and O. K. Andersen, Improved tetrahedron method for Brillouin-zone integrations, Phys. Rev. B **49**, 16223 (1994).

[43] N. A. Smirnov, Ab initio calculations of the elastic and thermodynamic properties of gold under pressure, J. Phys.: Condens. Matter **29**, 105402 (2017).

[44] K.-H. Hellwege and O. Madelung (Eds.), *Phonon States of Elements. Electron States and Fermi Surfaces of Alloys*, Landolt-Börnstein, New Series, Group III, Vol. 13 Pt. a (Springer, Berlin, 1981).

[45] J. Bass and K. H. Fischer, *Metals: Electronic Transport Phenomena*, edited by K.-H. Hellwege and J. L. Olsen, Landolt-Börnstein, New Series, Group III, Vol. 15, Pt. a (Springer-Verlag, Berlin, 1982).

[46] P. G. Klemens, G. Neuer, B. Sundqvist, C. Uher, and G. K. White, *Metals: Electronic Transport Phenomena*, edited by O. Madelung and G. White, Landolt-Börnstein, New Series, Group III, Vol. 15, Pt. c (Springer-Verlag, Berlin, 1991).

[47] V. E. Zinoviev, Thermophysical properties of metals at high temperatures (Metallurgy, Moscow, 1989) [in Russian].

[48] C. Y. Ho, R. W. Powell, P. E. Liley, Thermal Conductivity of the Elements, J. Phys. Chem. Ref. Data **1**, 279 (1972).

[49] L. Binkele, Significance of discrete Lorenz function levels at high temperatures resulting from new metallic conductivity measurements, High Temp.- High Press. **18**, 599 (1986).

[50] H.-J. Güntherodt, E. Hauser, H. U. Kunzi, R. Muller, The electrical resistivity of liquid Fe, Co, Ni, Pd, Phys. Lett. A **54**, 291 (1975).

[51] M. J. Laubitz, T. Matsumura, High-temperature transport properties of palladium, Can. J. Phys. **50**, 196 (1972).

[52] W. B. Holzapfel, M. Hartwig, W. Sievers, Equations of state for Cu, Ag, and Au for wide ranges in temperature and pressure up to 500 GPa and above, J. Phys. Chem. Ref. Data **30**, 515 (2001).

[53] J. W. Arblaster, Crystallographic properties of palladium, Platinum Met. Rev. **56**, 181 (2012).

[54] A. P. Cracknell, *Metals: Phonon States of Elements. Electron States and Fermi Surfaces*, edited by K.-H. Hellwege and J. L. Olsen, Landolt-Börnstein, New Series, Group III, Vol. 13, Pt. c (Springer-Verlag, Berlin, 1984).

[55] B. V. Vlasov, S. G. Taluts, V. E. Zinov'ev, N. A. Korenovskii, V. P. Polyakova, Kinetic properties of iridium, rhodium, palladium, and platinum in solid and liquid states, Fiz. Met. Metallogr. **10**, 89 (1992) [Phys. Met. Metallogr. **74**, 371 (1992)].

[56] E. G. Gamaly, The physics of ultra-short laser interaction with solids at non-relativistic intensities, Phys. Rep. **508**, 91 (2011).

[57] F. Bottin, G. Zerah, Formation enthalpies of monovacancies in aluminum and gold under the condition of intense laser irradiation, Phys. Rev. B **75**, 174114 (2007).

[58] D. V. Minakov, P. R. Levashov, Melting curves of metals with excited electrons in the quasiharmonic approximation, Phys. Rev. B **92**, 224102 (2015),

[59] V. Recoules, J. Clérouin, G. Zérah, P. M. Anglade, S. Mazevet, Effect of Intense Laser Irradiation on the Lattice Stability of Semiconductors and Metals, Phys. Rev. Lett. **96**, 055503 (2006).

[60] D. V. Knyazev, P. R. Levashov, Transport and optical properties of warm dense aluminum in the two-temperature regime: *Ab initio* calculation and semiempirical approximation, Phys. Plasmas **21**, 073302 (2014).

[61] D. S. Ivanov, L. V. Zhigilei, Combined atomistic-continuum modeling of short-pulse laser melting and disintegration of metal films, Phys. Rev. B **68**, 064114 (2003).

[62] B. Rethfeld, D. S. Ivanov, M. E. Garcia, S. I. Anisimov, Modelling ultrafast laser ablation, J. Phys. D: Appl. Phys. **50**, 193001 (2017).